Oil Shale, 2024, Vol. 41, No. 2, pp. 77–102
doi: https://doi.org/10.3176/oil.2024.2.01
ISSN 0208-189X

Exploring the influence of effective stress sensitivity on oil shale: implications for porosity and permeability

Dandan Lu[a], Yao Cheng[a,b]*, Longfei Zhao[c]

[a] School of Mechanics and Engineering, Liaoning Technical University, Fuxin 123000, China
[b] College of Innovation and Practice, Liaoning Technical University, Fuxin 123000, China
[c] Tuha Drilling Company of CNPC Xibu Drilling Engineering Company Limited, Xinjiang 838200, China

Received 10 November 2023, accepted 19 April 2024, available online 30 April 2024

Abstract. *Changes in the porosity and permeability of oil shale under the overburden pressure often have a significant impact on the subsequent development of reservoirs. The authors of this article investigated the overburden porosity and permeability characteristics of tight oil reservoirs in two regions in China: the Fushun West Open-pit Mine in Liaoning and the Jimsar shale oilfield in Xinjiang. Overburden porosity and permeability experiments were conducted on oil shale cores. Three-dimensional visualization and quantitative analysis of the micropore structure of cores under different effective stresses were used to model the relationship between oil shale porosity, permeability, and effective stress. In addition, the stress sensitivity of oil shale reservoirs was analyzed, using the damage rates of permeability and stress sensitivity coefficients. The results indicated that in both regions, oil shale porosity and permeability exhibited a decreasing trend with increasing effective stress, following a negative exponential function. When the effective stress was less than 8 MPa, the permeability stress sensitivity coefficient decreased sharply. Once the effective stress exceeded 8 MPa, the stress sensitivity of permeability in both regions weakened, maintaining a range between 0.2 and 0.4 MPa^{-1}. The results of three-dimensional visualization simulations were the same as the experimental results. Taken together, the results showed that the porosity of different-sized pores decreased with increased stress, which reflected the synergistic effect of different-sized pores on porosity in shale. This study has practical significance for revealing the variation in pore size in shale reservoirs and establishing the physical characteristics of oil shale reservoirs.*

Keywords: *oil shale, porosity, permeability, stress sensitivity.*

* Corresponding author, yaoyao9873@163.com

1. Introduction

With the looming depletion of traditional energy sources, oil shale has gained prominence as a crucial strategic energy resource, due to its substantial reserves [1, 2], significant potential, and diverse utilization methods [3, 4]. Shale oil is a product of pyrolysis, formed through a series of physicochemical reactions, such as moisture volatilization, laminar thermal cracking, and casein pyrolysis. This results in the formation of pores and fractures within the rock matrix [5]. When fluid flows within the rock matrix, there is a highly complex interaction between the fluid and the rock. On one hand, changes in rock stress alter the characteristics of fluid flow; on the other hand, changes in fluid flow characteristics further modify the rock stress field. With increasing stress, the permeability and porosity of porous media decrease. When extracting oil and gas, the decline in pore pressure coupled with the generation of internal fluids disrupts the original stress equilibrium, leading to elastic or plastic rock deformations. Consequently, changes in pore structure and volume also affect the permeability of porous media. The purpose of stress sensitivity testing is to understand the deformation process of pores and throats; i.e., how cracks open or close with changes in net stress, thereby causing variations in rock permeability. Stress sensitivity refers to the compression of porous media [6]. Changes in pore structure and volume significantly influence reservoir porosity and permeability, ultimately affecting fluid flow and production dynamics in reservoirs [7]. Notably, numerous studies have demonstrated that the stress sensitivity of permeability is far more significant than that of porosity [8].

Since Biot [9] proposed the relationship between effective stress and permeability, a series of permeability experiments have been conducted on various rocks over the subsequent decades to study the evolution of permeability and porosity with stress variations. For instance, Snow [10], Jones [11], McKee et al. [12], Liu and Liu [13], and Chang et al. [14], among others, utilized various experimental equipment and methods to reveal that under the coupling effect of fluid–solid seepage, the permeability of rocks is not fixed but rather a function of the effective stress of the rock mass. These researchers independently summarized empirical formulas describing the relationship between rock permeability characteristics and effective stress. Various empirical and theoretical models have been proposed to characterize the stress sensitivity of permeability and porosity. Examples include Walsh's [15] natural logarithm model, Shi and Wang's [16] power-law model, Katsube et al.'s [17] exponential function model, Kwon et al.'s [18] cubic law model, and Zheng et al.'s [19] two-part Hookean model.

Brower and Morrow [20] attributed the stress sensitivity of permeability to high aspect ratio pores. Li et al. [21] observed that the stress sensitivity of low-rank coal pore volume is primarily controlled by microcracks and cleats. For medium- to high-rank coals, micropores, mesopores, and macropores exhibit higher sensitivity to stress. Chalmers et al. [22] found

that the permeability parallel to the bedding is more sensitive to stress than the permeability perpendicular to the bedding. Ghanizadeh et al. [23] and Gensterblum et al. [24] reported higher stress sensitivity in shale pore systems when water is present. After conducting stress sensitivity experiments on coal samples from different regions, coal ranks, and water saturation levels, researchers evaluated and analyzed their stress sensitivity and mechanisms. Non-linear fitting has been performed in several studies, using logarithmic, power-law, and polynomial expressions to describe the variation of coal rock permeability with stress [25–29]. Ostensen [30] found in confined pressure tests that the loading rate of axial stress and confining pressure affect the results of stress sensitivity experiments. Li et al. [31] suggested that low-permeability tight reservoirs exhibit low stress sensitivity. Dou et al. [32] found a correlation between the results of confining pressure and variable backpressure experiments, suggesting their mutual convertibility. Feng et al. [33] established a theoretical predictive model for crack permeability under different conditions, based on the linear elastic theory. The relative error between theoretical predictions and numerical simulations was less than 10%. The fundamental reason for stress sensitivity in fractured reservoirs was found to be changes in the geometric shape of fractures and mineral deformation. Facing difficulties measuring permeability in tight rock cores, Chen et al. [34] applied pulse decay permeability measurement methods to stress sensitivity measurements. Zhao et al. [35] evaluated conventional stress sensitivity, using microcrack cores and matrix cores, concluding that the stress sensitivity of microcrack cores is stronger than that of matrix cores.

Currently, researchers both domestically and internationally have made certain progress in the study of stress sensitivity in rock permeability. However, most of the research has been focused on conventional reservoirs [36–39]. There is relatively little research on the stress sensitivity of unconventional reservoirs [40]. Microscopic pore structures, such as the shape and size of pores and throats, influence the stress sensitivity of reservoir permeability [41]. Many scholars have studied the impact of permeability stress sensitivity on reservoir development through experimental, theoretical, and numerical simulation methods [42]. Stress sensitivity significantly affects the development of oil and gas reservoirs [43]. In foreign research, David et al. [44] elucidated an exponential equation for the stress sensitivity coefficient, which can be divided into a porosity sensitivity index and porosity compressibility. Their exponential equation provides a method to link the external properties of rocks with their internal characteristics. The porosity compressibility index describes the relationship between porosity and permeability, and porosity compressibility reflects the compressibility characteristics of reservoirs [45]. Mavko and Nur [46] established a porosity compressibility formula, based on the spindle-shaped fracture model. In domestic studies, Zhang et al. [47] found that the compressibility of elliptical and circular pores is related to the mechanical parameters of rocks and the

geometric structure of pores. Considering the different pore structures of shale, Zhang et al. [48] simplified the pore structure model of shale, proposing a dual-porosity model that considers matrix pores and microcracks, and used the porosity sensitivity index to reflect stress sensitivity. However, the influence of porosity compressibility was overlooked [49]. Previous studies have shown that the relationship between stress sensitivity and pore structure in oil shale is not clearly understood. To delve deeper into this relationship, it is crucial to employ three-dimensional visualization simulation methods that intuitively present the changes in the internal pore structure of oil shale under different stress conditions. This comprehensive simulation analysis will contribute to a better understanding of the impact of stress on the pore characteristics of oil shale, providing specific visual guidance for interpreting the mechanical behavior of oil shale.

To investigate the stress sensitivity of oil shale, this study employed experimental methods to determine the stress sensitivity of porosity and permeability in oil shale samples under overburden conditions. A model of the relationship between porosity, permeability, and effective stress in oil shale was established. Specifically, X-ray micro-computed tomography (μCT) technology was utilized for three-dimensional visualization and simulation reconstruction analysis of oil shale samples. The simulation results were consistent with the experimental results, revealing the stress sensitivity changes in porosity and permeability. This comprehensive approach, combining experiments with simulations, provides crucial insights for a deeper understanding of the stress sensitivity of oil shale.

2. Materials and methods

2.1. Preparation of oil shale samples

The Fushun West Open-pit Mine is located in Fushun City, Liaoning Province, China, and is one of the earliest developed oil shale-producing areas in China, renowned for its abundant oil shale resources. Similarly, the Jimsar shale oilfield is situated in the central-western part of the Xinjiang Uygur Autonomous Region, belonging to the Tarim Basin. It is another important oil shale-producing area in China. These two regions share similarities in terms of geographical location, resource type, and development history. They play crucial roles in the development of oil shale and shale gas in China, constituting key components of the domestic energy industry. Shale formations typically exhibit lower permeability, making it challenging for oil to flow within reservoirs. This increases the difficulty of oil extraction, necessitating enhanced recovery techniques, such as horizontal drilling and hydraulic fracturing, to improve oil production rates. During the fracturing process, the stress sensitivity of porosity and permeability in shale formations

Fig. 1. Oil shale samples: (a), (b) Fushun West Open-pit Mine; (c), (d) Jimsar, Xinjiang.

plays a crucial role in hydraulic fracturing and subsequent extraction. In this study, experimental samples were collected from the Fushun West Open-pit Mine and the Jimsar region in Xinjiang, considering the influence of shale heterogeneity. Rocks from the same profile were selected to prepare four experimental samples (Fig. 1). The rock samples were cylindrical in shape (diameter 2.47–2.52 cm, length 2.48–2.54 cm). To thoroughly remove any potential moisture and ensure the samples are in a dry state without affecting the experimental results, the test samples were continuously oven-dried at 60 °C for 48 hours [50, 51]. At this temperature, continuous oven-drying effectively eliminates moisture from the samples, while avoiding potential impacts on the sample structure due to high temperatures. This processing method aims to preserve the samples in their original state as much as possible, ensuring more reliable experimental results.

2.2. Experimental instruments and methods

This experiment utilized the AP-608 automated permeameter-porosimeter (Fig. 2) to measure the permeability and porosity of rocks under reservoir pressure conditions. The AP-608 experimental apparatus employs the gas pulse decay method for measurements, allowing for the determination of the gas-phase permeability and porosity of rocks under actual reservoir pressure conditions. It can also ascertain the equivalent liquid and air-phase relative permeability, porosity, and pore volume. The AP-608 features a user-friendly visual operating interface that allows direct observation of the testing process. It provides the flexibility to choose permeability testing, porosity testing, and simultaneous porosity and permeability testing, and enables testing at multiple pressure points on a single rock sample as needed. The instrument's pore pressure ranges from 100 to 250 psi, confining pressure ranges from 500 to 9500 psi, permeability testing spans from 0.001 to 10,000 mD, and porosity testing covers a range from 0.1% to 40%. High-pressure air was used as the confining pressure gas source during the experiment, and high-purity helium gas was employed for testing purposes.

Fig. 2. AP-608 automated permeameter-porosimeter.

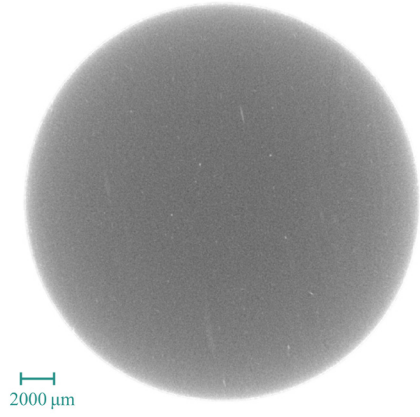

Fig. 3. Unpressurized CT scan image of oil shale.

To investigate the impact of overburden on the porosity and permeability of oil shale, overburden pressure was increased to simulate variation in effective stress in the geological formation. Measurements were taken to observe how the porosity and permeability of oil shale changed with varying confining pressure. In this way, the relationship between stress changes and shale porosity and permeability was analyzed. The confining pressures were set at 4, 6, 8, 10, 12, 14 and 17 MPa, each maintained for a duration of at least 30 minutes. A pulse pressure of 1 MPa was applied to determine the gas permeability at each stress point. During real-time measurements, the applied pressure did not exactly match the pore pressure, which exhibited minor fluctuations within reasonable limits.

Following the overburden process, the pore structure of oil shale samples was scanned and analyzed using µCT (Fig. 3). This analysis revealed the correlating factors of porosity and permeability under different stress sensitivities. Specifically, the µCT technology was employed for three-dimensional reconstruction, enabling a high-precision observation of the microscopic structure of rock samples, including the pore size, distribution, and interrelationships. This method allowed for an in-depth understanding of the impact of overburden on oil shale porosity, with the aim of providing insight into the microscopic changes in pore structure and permeability. Through this analytical approach, it was possible to identify the direct and indirect effects of stress changes on porosity and permeability. Beyond quantitative measurements, a three-dimensional visualization of the pore structure facilitated the exploration of the response mechanisms of shale rocks at the microscopic level.

3. Results and discussion

To compare the differences in the stress sensitivity of porosity and permeability in the oil shale reservoirs in Fushun and Xinjiang, models of porosity and permeability functions were used to fit parameters such as the stress sensitivity coefficient, porosity and permeability damage rates, porosity compressibility coefficient, permeability stress sensitivity coefficient. A comprehensive comparative analysis was conducted on the stress sensitivity of porosity and permeability in oil shale.

3.1. Relationship of porosity, permeability, and stress in oil shale

The Terzaghi equation was used to calculate the effective stress in the overburdened permeability experiment of oil shale samples [52]:

$$\sigma_{eff}^{T} = \sigma - P, \tag{1}$$

where σ is the confining pressure applied to the sample, MPa; P is the fluid pressure during the sample test, MPa; and σ_{eff}^{T} is the Terzaghi effective stress during the experimental process.

The relationship between the porosity, permeability, and effective stress of oil shale under overburden pressure is illustrated in Figure 4.

(a)

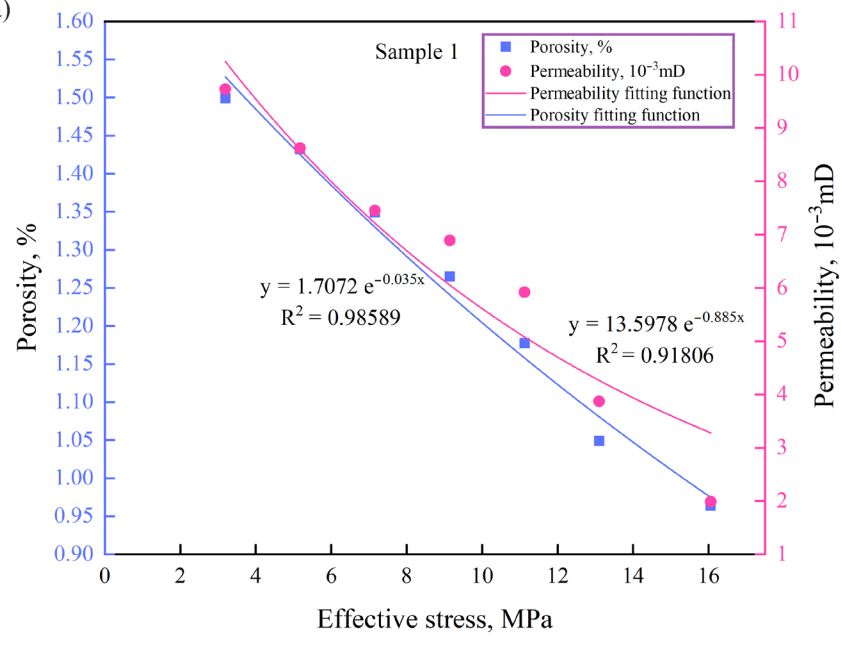

(b)

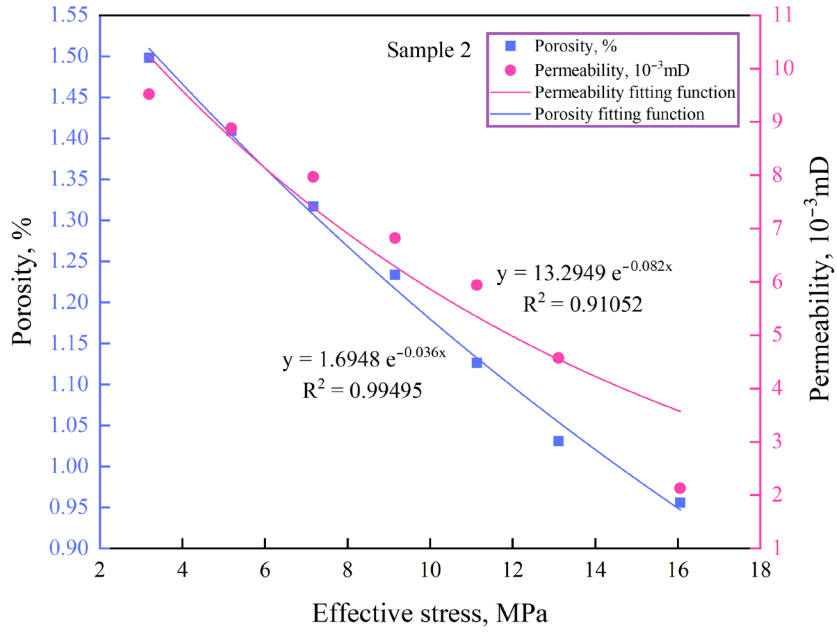
Sample 2
Porosity, %
Permeability, 10⁻³mD
Permeability fitting function
Porosity fitting function
y = 13.2949 e^-0.082x
R² = 0.91052
y = 1.6948 e^-0.036x
R² = 0.99495
Porosity, %
Permeability, 10⁻³mD
Effective stress, MPa

(c)

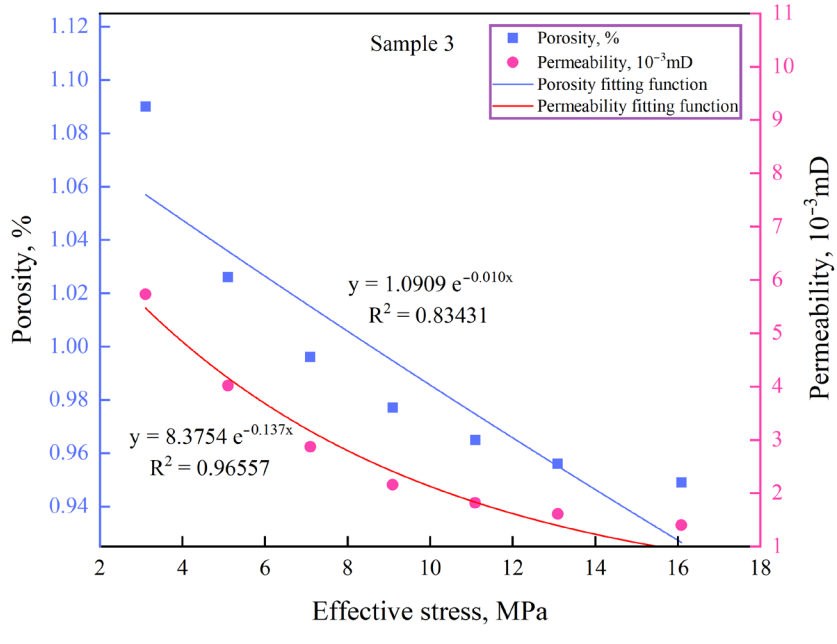
Sample 3
Porosity, %
Permeability, 10⁻³mD
Porosity fitting function
Permeability fitting function
y = 1.0909 e^-0.010x
R² = 0.83431
y = 8.3754 e^-0.137x
R² = 0.96557
Porosity, %
Permeability, 10⁻³mD
Effective stress, MPa

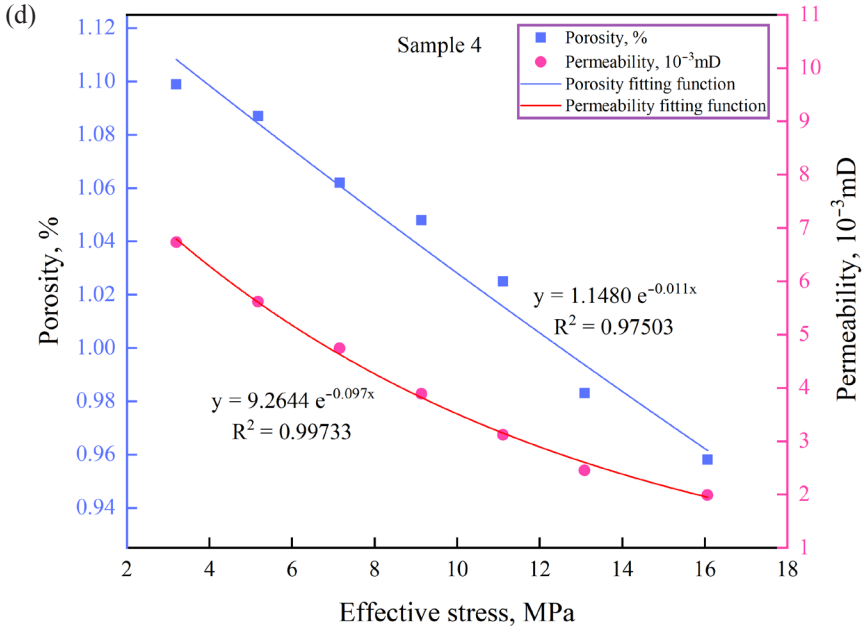

Fig. 4. Relationship between the porosity, permeability and effective stress of oil shale under overburden pressure.

The two oil shale samples from the Fushun area are denoted as samples 1 and 2, and the two oil shale samples from the Xinjiang area are denoted as samples 3 and 4. As shown in Figure 4, there is a good correlation among porosity, permeability, and effective stress in the oil shale specimens from Fushun. In contrast, the correlation between porosity, permeability, and effective stress is slightly weaker in the oil shale specimens from Xinjiang.

The relationship between oil shale rock porosity and effective stress is a negative exponential function; i.e., the porosity of oil shale reservoir decreases with increasing effective stress. Regression analysis of the experimental results yields the following relationship:

$$\varphi_i = \varphi_0 e^{-C_p P}, \tag{2}$$

where φ_i is the porosity under a given pressure condition, %; P is the effective stress value from the initial to a given pressure state, MPa; φ_0 is the porosity when the initial pressure is 0, %; and C_p is the compression coefficient of shale reservoir, MPa^{-1}.

The experimental results of porosity for the four samples under overburden conditions are shown in Table 1. For the oil shale in the Fushun West Open-pit Mine area, the initial porosity (φ_0) ranges from 1.6948% to 1.7072%, with an average of 1.701%. The corresponding compression coefficients are in the

range of 0.35 to 0.36 MPa^{-1}, with an average of 0.355 MPa^{-1}. This indicates that oil shale in this region has a relatively high initial porosity and compression coefficient, which may reflect the influence of geological conditions on the physical properties of rocks in this area. In the Jimsar region of Xinjiang, the initial porosity (φ_0) of oil shale ranges from 1.0909% to 1.1480%, with an average of 1.1194%. The compression coefficient is in the range of 0.010 to 0.011 MPa^{-1}, with an average of 0.0105 MPa^{-1}. In comparison to the oil shale in Fushun, the oil shale in Xinjiang shows lower values in terms of initial porosity and the compression coefficient, possibly due to differences in geological environments.

The gas permeability of the oil shale samples follows a negative exponential function with effective stress. As the effective stress increases, the permeability of oil shale samples decreases according to the negative exponential law. The relationship is expressed as an exponential decrease:

$$K_i = K_0 \, e^{-aP}, \tag{3}$$

where K_i is the permeability under a given pressure, $\times 10^{-3}$ mD; P is the effective stress value from the initial to a given pressure state, MPa; K_0 is the permeability when the initial pressure is 0, $\times 10^{-3}$ mD; and a is the permeability stress sensitivity coefficient, MPa^{-1}.

By analyzing the results of the permeability experiment of oil shale samples under the overlying conditions (Table 1), the following trends can be observed. The initial permeability (K_0) of oil shale in Fushun ranges from 13.5978 to 13.2949 × 10^{-3} mD, with an average of 13.4463 × 10^{-3} mD. The stress sensitivity coefficient ranges from 0.885 to 0.082 MPa^{-1}, with an average value of 0.4835 MPa^{-1}. Comparatively, the initial permeability (K_0) of oil shale in the Jimsar area of Xinjiang ranges from 8.3754 to 9.2644 × 10^{-3} mD, with an average of 8.8199 × 10^{-3} mD, while the stress sensitivity coefficient varies within the range of 0.137 to 0.097 MPa^{-1}, with an average of 0.117 MPa^{-1}. These data reveal different responses in permeability under overburden conditions for the oil shale in the two regions. The oil shale in Fushun exhibits relatively higher values of both the initial permeability and the stress sensitivity coefficient, indicating a more significant influence during the overburden process. In contrast, the oil shale in Jimsar shows lower values of both the initial permeability and the stress sensitivity coefficient, suggesting relatively minor changes in permeability under the same overburden conditions.

Table 1. Statistical analysis of the porosity, permeability and effective stress of oil shale samples

Sample ID	Compression coefficient (C_p), MPa^{-1}	Porosity (φ_0), %	Correlation coefficient (R^2_1)	Permeability stress sensitivity coefficient (a), MPa^{-1}	Permeability (K_0), 10^{-3} mD	Correlation coefficient (R^2_2)
1	0.035	1.7072	0.98589	0.885	13.5978	0.91806
2	0.036	1.6948	0.99495	0.082	13.2949	0.91052
3	0.010	1.0909	0.83431	0.137	8.3754	0.96557
4	0.011	1.1480	0.97503	0.097	9.2644	0.99733

3.2. Porosity stress sensitivity

The porosity damage rate ($D\varphi$) refers to the extent of damage to the formation or rock porosity under certain conditions. A higher $D\varphi$ indicates that the reservoir porosity is more susceptible to the influence of stress, and thus has a higher degree of stress sensitivity. If $D\varphi$ is a positive value, this indicates a decrease in porosity and hence porosity damage. If $D\varphi$ is a negative value, this indicates an increase in porosity and hence porosity recovery or expansion. The formula is as follows:

$$D_\varphi = \frac{\varphi_1 - \varphi_i}{\varphi_1} \times 100\%, \tag{4}$$

where $D\varphi$ is the porosity damage rate, %; φ_1 is the initial stress point porosity, MPa; and φ_i is the porosity of the i-th pressure point, MPa. Under the same confining pressure condition, the higher the porosity damage rate, the higher the stress sensitivity of the oil shale reservoir. The strength of the oil shale porosity damage rate is divided according to the experimental evaluation method of reservoir sensitivity (SY/T 5358-2010) [53] (see Table 2).

Table 2. Evaluation index of the porosity damage rate

Porosity damage rate, %	$D\varphi \leq 5$	$5 < D\varphi \leq 30$	$30 < D\varphi \leq 50$	$50 < D\varphi \leq 70$	$D\varphi > 70$
Degree of damage	–	Weak	Moderate to weak	Medium to strong	Strong

The porosity damage rate of oil shale in the Fushun region ranges from 4.47% to 36.18%, while in the Xinjiang region, it varies between 1.09% and 12.94%. This indicates that both regions exhibit relatively weak degrees of

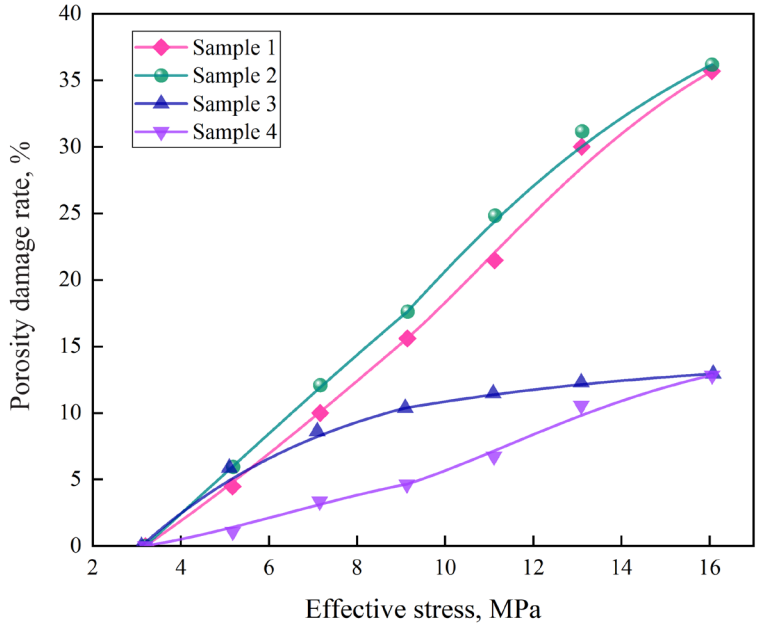

Fig. 5. Relationship between the porosity damage rate and effective stress.

porosity damage (Fig. 5). Specifically, the porosity damage rate of oil shale in the Fushun region gradually increases with more effective stress. In contrast, the variation in Xinjiang is relatively small. This observation suggests that the porosity structure of oil shale in the Fushun region may be more susceptible to significant damage under the influence of increasing effective stress. This could be related to the geological conditions and rock properties in the Fushun region, making oil shale more vulnerable to external stress, and resulting in damage to the porosity structure. Conversely, the oil shale in Xinjiang exhibits a relatively lower porosity damage rate under similar conditions, indicating a certain resistance to stress-induced damage in the rocks of that region.

In the experimental analysis of oil shale porosity, permeability, and their stress sensitivity, the porosity compressibility coefficient is crucial. This coefficient directly reflects the compressibility characteristics of the rock's porosity structure under changes in external stress. The magnitude of the porosity compressibility coefficient is directly related to the sensitivity of the rock porosity structure to stress, indicating the extent of porosity structure changes under stress. For oil shale, a high porosity compressibility coefficient suggests that the porosity structure is more susceptible to stress, potentially leading to significant changes in porosity. Therefore, when studying porosity, permeability, and stress sensitivity, comprehensive consideration of the porosity compressibility coefficient is essential to ensure a thorough understanding of the rock's response behavior. The porosity compressibility coefficient is defined as follows:

$$C_p = -\frac{1}{\phi_0}\left(\frac{\partial \phi}{\partial P}\right)_T, \quad (5)$$

where C_p is the pore compression coefficient of shale reservoir, MPa^{-1}; ϕ_0 is the porosity under the initial effective stress, %; and $(\partial\phi / \partial P)_T$ is the change rate of oil shale porosity with effective stress under isothermal conditions, MPa^{-1}.

With increased effective stress, the oil shale samples from Fushun and Xinjiang exhibit a two-stage pattern in the porosity compressibility coefficient (Fig. 6). The first stage is the initiation of microcracks, and with the increase of effective stress, the oil shale sample initially forms microcracks. In this stage, the porosity compressibility coefficient decreases sharply, showing stronger stress sensitivity. The second stage is the closure of microcracks, and with the gradual increase in pressure, the pores of the oil shale sample gradually close. In this stage, the curve of the porosity compressibility coefficient tends to stabilize, indicating weaker stress sensitivity.

In the oil shale samples from Fushun, when the effective stress is less than 7 MPa, the porosity compressibility coefficient decreases sharply, from 0.4 to 0.15 MPa^{-1}, dropping by approximately 62.5%. However, once the effective stress exceeds 7 MPa, the porosity compressibility coefficient increases slowly. In contrast, the oil shale samples from Xinjiang show an upward and downward trend in the porosity compressibility coefficient when the effective stress is less than 10 MPa. However, once the effective stress exceeds 10 MPa, the porosity compressibility coefficient stabilizes and remains at a relatively low level, below 0.1 MPa^{-1}.

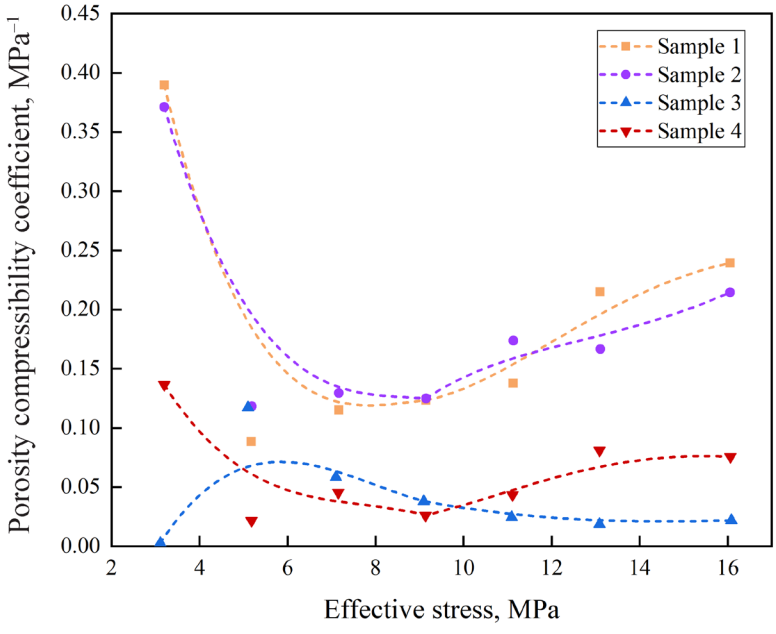

Fig. 6. Relationship between the porosity compressibility coefficient and effective stress.

3.3. Permeability stress sensitivity

Rock in oil shale formations is a porous medium composed of various substances, including mineral particles, mud, and cementing materials. Under compression conditions, these materials undergo different deformations, and the degree of compression varies for different types of substances. To evaluate the stress sensitivity of permeability in oil shale formations, based on previous research on stress sensitivity and relevant industry standards, two main parameters are used to assess the confining pressure sensitivity of permeability in oil shale.

The permeability damage rate reflects the percentage of reservoir permeability damage under effective stress:

$$D_K = \frac{K_1 - K_n}{K_1} \times 100\% , \tag{6}$$

where D_K is the maximum permeability compression rate, %, generated in the process of stress increasing to the maximum; K_1 is the permeability of the rock sample at the first stress point under recompression, $\times 10^{-3}$ mD; and K_n is the permeability at an effective stress, $\times 10^{-3}$ mD. According to the evaluation criteria provided by the evaluation method of reservoir sensitivity flow experiment [53], the permeability damage degree of coal samples of different coal grades was evaluated.

Table 3. Evaluation index of permeability damage rate

Permeability damage rate, %	$D_K \leq 5$	$5 < D_K \leq 30$	$30 < D_K \leq 50$	$50 < D_K \leq 70$	$D_K > 70$
Degree of damage	–	Weak	Moderate to weak	Medium to strong	Strong

With a gradual increase in effective stress, the permeability damage rate of experimental oil shale shows a significant upward trend (Fig. 7). Specifically, within the range of effective stress less than 9 MPa, the permeability damage rate increases sharply. In the range of effective stress between 9 and 16 MPa, the growth rate of the damage rate slows down slightly. Beyond an effective stress of 16 MPa, the permeability damage rate tends to stabilize. This observation indicates that at lower stress levels, the permeability of oil shale undergoes significant damage, likely due to the compression and deformation of the pore structure. As stress further increases, the growth rate of the damage rate slows down gradually, eventually reaching a relatively stable state. This may reflect that under high-stress conditions, the pore structure of the rock undergoes significant changes, leading to a more gradual variation in permeability.

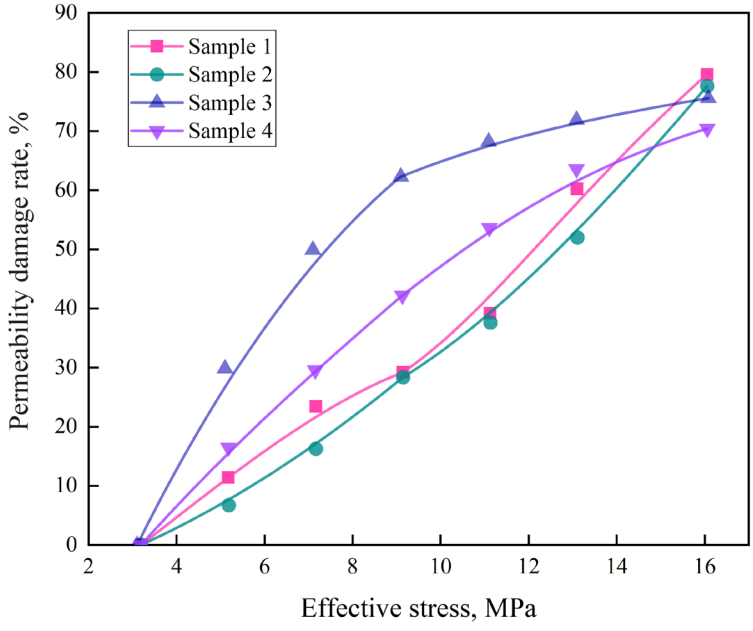

Fig. 7. Relationship between the permeability damage rate and effective stress.

Due to the uniqueness of rock structures, the discontinuity of mechanical properties, and the complexity of the coupled interaction between stress and flow fields during the permeation process, the mechanism is still under study. The influencing factors of rock permeability are comprehensive, and the process is complex, making it difficult to describe each factor individually. It is possible to consider defining a sensitivity coefficient α_k of rock permeability to effective stress. By defining such a coefficient, the factors influencing rock permeability are normalized. The permeability stress sensitivity coefficient is defined as follows:

$$\alpha_k = -\frac{1}{K_0} \times \frac{\partial K}{\partial P} \ , \tag{7}$$

where K_0 represents the permeability under initial effective stress, $\times 10^{-3}$ mD; ∂K is the change in permeability, $\times 10^{-3}$ mD; and ∂P is the change in pressure, MPa. The sensitivity coefficient α_k reflects the trend of rock permeability with changes in effective stress. A higher α_k value indicates greater sensitivity of rock permeability to changes in effective stress, while a lower value suggests smaller sensitivity. Thus, determining the values of rock permeability under different effective stresses is transformed into the determination of its sensitivity coefficient α_k. Based on Equation (7), if the effective stress changes from P_0 to P, then the rock permeability at this moment is as follows:

$$K = K_0(1 - \int_{P_0}^{P} \alpha_k \mathrm{d}P) \ . \tag{8}$$

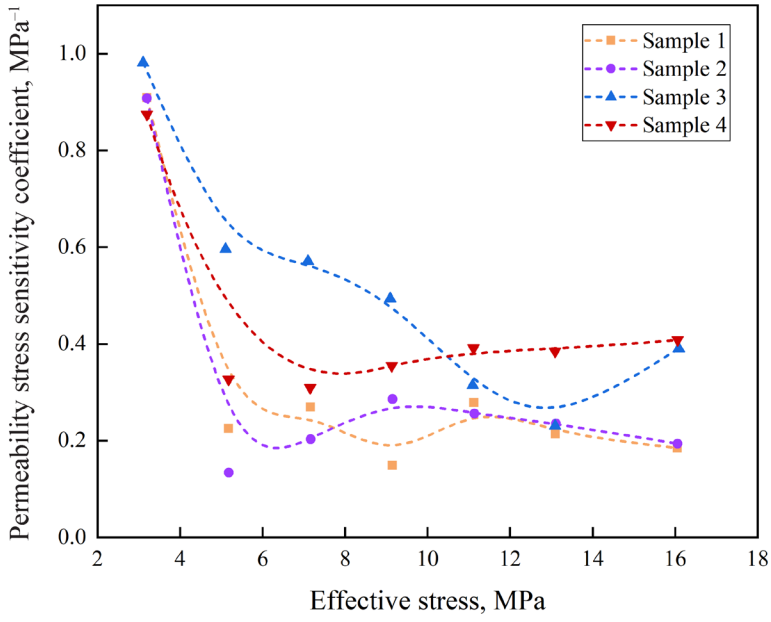

Fig. 8. Relationship between the permeability stress sensitivity coefficient and effective stress.

As the effective stress gradually increases, the trends of the permeability stress sensitivity coefficients in the oil shale samples from Fushun and Xinjiang show nearly identical patterns (Fig. 8). In the oil shale samples from the Fushun region, when the effective stress is less than 8 MPa, the permeability stress sensitivity coefficient decreases sharply, reaching approximately 0.4 MPa^{-1}. In contrast, in the Xinjiang oil shale samples, when the effective stress is below 8 MPa, the permeability stress sensitivity coefficient drops sharply to around 0.2 MPa^{-1}. Once the effective stress exceeds 8 MPa, the permeability stress sensitivity coefficient curves gradually flatten in both regions, maintaining values between 0.2 and 0.4 MPa^{-1}.

3.4. Relationship between porosity and permeability

The relationship between porosity and permeability in oil shale holds significant importance in rock mechanics and the development of oil shale resources. Generally, there is a positive correlation between porosity and permeability, but the specific relationship is influenced by various factors. In order to capture the complexity of internal pore structures in rocks and provide an intuitive indicator for studying pore characteristics, the logarithm of the ratio of permeability under certain pressure conditions (K_i) to initial permeability (K_0) is taken for dimensionless representation: $\ln(K_i/K_0)$. Similarly, the logarithm of the ratio of porosity under certain pressure conditions (φ_i) to

initial porosity (φ_0) is taken for dimensionless representation: $\ln(\varphi_i/\varphi_0)$ [26–28]. With the increase of dimensionless $\ln(\varphi_i/\varphi_0)$, dimensionless $\ln(Ki/K_0)$ also increases, and its relationship satisfies a linear correlation:

$$\ln(K_i/K_0) = \gamma \ln(\varphi_i/\varphi_0) + m\,, \tag{9}$$

where γ is introduced as the porous power index, indicating the ratio of matrix to fracture porosity; φ_i is the porosity under a given pressure, %; and K_i is the permeability at a given pressure, $\times 10^{-3}$ mD.

First, the relatively lower γ-values of the Fushun oil shale suggest that its pore structure may be dominated by matrix-type pores. The average γ-value of the oil shale samples from the Fushun region is approximately 3.083, with a maximum value of 3.257 (Fig. 9). This indicates that matrix-type pores dominate the overall pore structure. These pores may be relatively small, contributing relatively less to the overall permeability. In contrast, the higher γ-values of the Xinjiang oil shale indicate that its pore structure may be more complex, with more developed fracture-type pores. The average γ-value of the oil shale samples from the Xinjiang region is around 9.469, with a maximum value of 10.298. This suggests that fracture-type pores have a significant impact on the overall pore structure. These pores may be larger, exerting a more pronounced influence on the overall permeability.

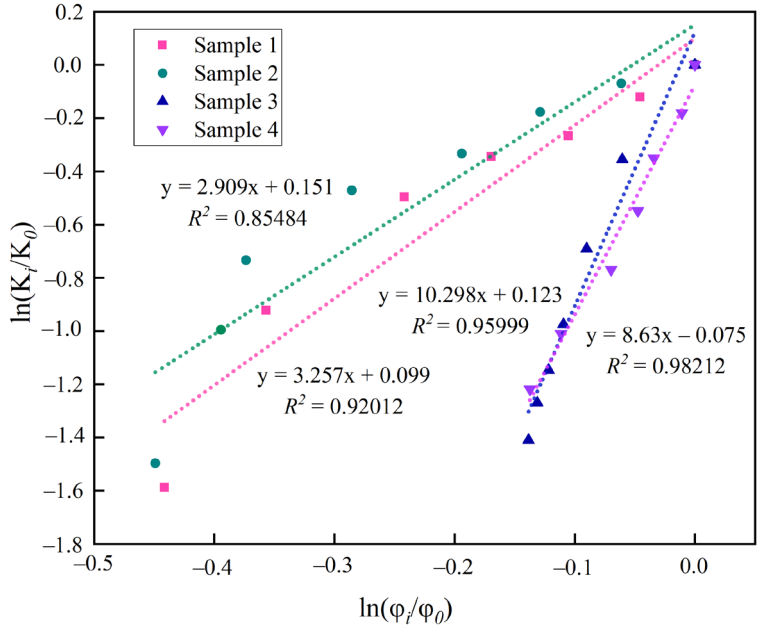

Fig. 9. Double logarithmic pore permeability curve of oil shale under overlying pressure.

Second, these numerical results may reflect differences in the maturity and composition of the shale samples between the two regions. Higher γ-values are often associated with more mature shale, as an increase in maturity may be accompanied by the development of more fracture-type pores. In this regard, the higher average γ-values in the Xinjiang region may reflect a relatively higher level of maturity in the shale samples from that area. In cases with higher γ-values, fracture-type pores may be more developed, potentially consisting of small and densely distributed fractures with widths exceeding the pore radius of the matrix system. Due to the diversity of pore structures, pores intertwine at different scales and types, forming a comprehensive pore network. Therefore, even when an overall decrease in porosity and permeability is observed, the range of γ-values suggests the presence of a rich and variable pore structure within the rock.

3.5. Influence mechanism of pressure pore permeability change

After applying overburden pressure, CT scans were performed on the Fushun oil shale, and its pore structure was obtained through three-dimensional reconstruction (Fig. 10). Upon observation of the images, it was evident that with an increase in confining pressure, there was a gradual decrease in the number of pores. This phenomenon indicates that the effect of confining pressure causes closure or deformation of internal rock pores, resulting in an overall reduction in porosity. This change in pore structure is directly related to the permeability and reservoir properties of the rock. The reduction in pores is attributed to the close arrangement of rock particles, to the closure of microscopic cracks, or to the compression of fractures due to confining pressure. These changes have a significant impact on the gas permeability and reservoir capacity of oil shale, as the permeability of the rock is primarily influenced by its pore structure.

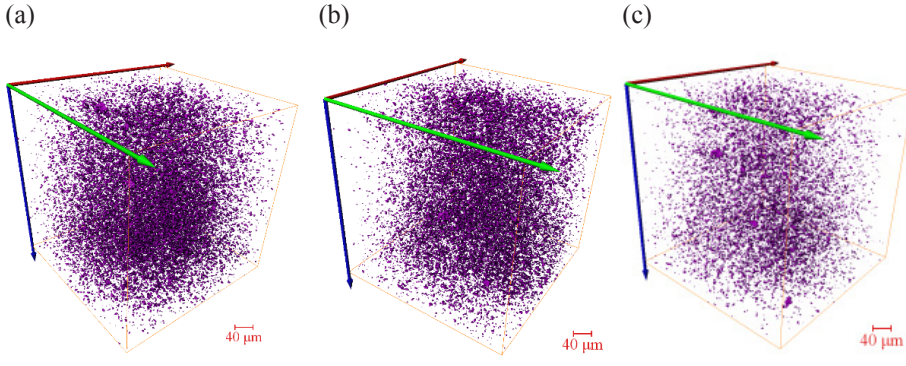

Fig. 10. Pore map of oil shale under overlying pressure: (a) 4 MPa, (b) 8 MPa, (c) 17 MPa.

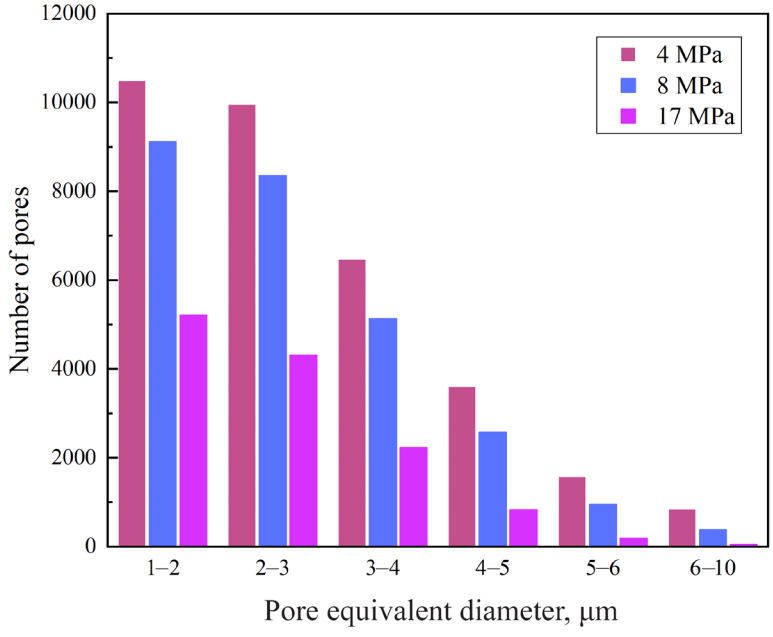

Fig. 11. Pore number of oil shale under different effective stresses.

A detailed analysis of the pore equivalent diameter distribution under different overlying conditions revealed significant changes in pore structure (Fig. 11). First, within the pore diameter range of 1–2 μm, there was a decreasing trend in the number of pores with an increase in overburden pressure. Specifically, under stress conditions ranging from 4 to 17 MPa, the number of pores decreased by approximately 13.2% and 50.4%, respectively. This result indicates that small-scale pores are significantly influenced by overburden pressure, potentially experiencing filling or closure. Secondly, in the range of 2–3 μm, the pore number decreased from 4 to 17 MPa by about 16.0% and 56.7%, respectively. In the range of 3–4 μm, the pore number decreased by about 20.6% and 65.6%, respectively. This again confirms that as the pore diameter increases, the number of pores affected by overburden pressure decreases. Additionally, for larger-scale pore diameter ranges (4–10 μm), the decreasing trend in the number of pores under different overburden conditions was more pronounced. In these ranges, compared to the rock samples without applied pressure, the pore numbers decreased by 76.8%, 85.4% and 94.3%, as the pressure increased from 4 MPa to 8 MPa and then to 17 MPa, respectively. These data highlight the closing effect of large pores in oil rocks under high stress conditions.

As effective stress increases, the pore area and volume of oil shale decrease noticeably. In the pore equivalent diameter range of 3–5 μm, the pore area and volume of oil shale were most concentrated. Under the high stress of

17 MPa, the pore area and volume of larger pores decreased considerably, showing a more pronounced reduction compared to the conditions at 4 MPa and 8 MPa (Fig. 12).

(a)

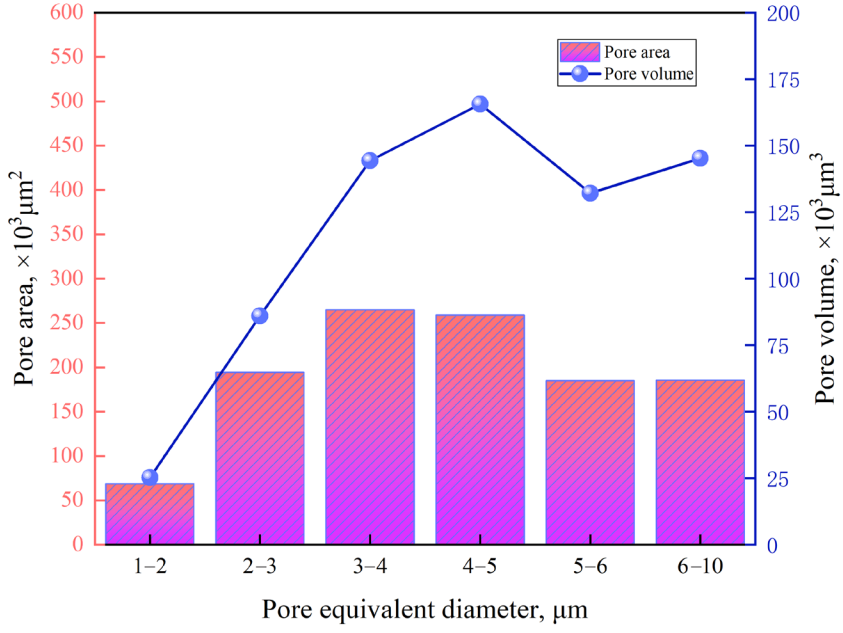

(b)

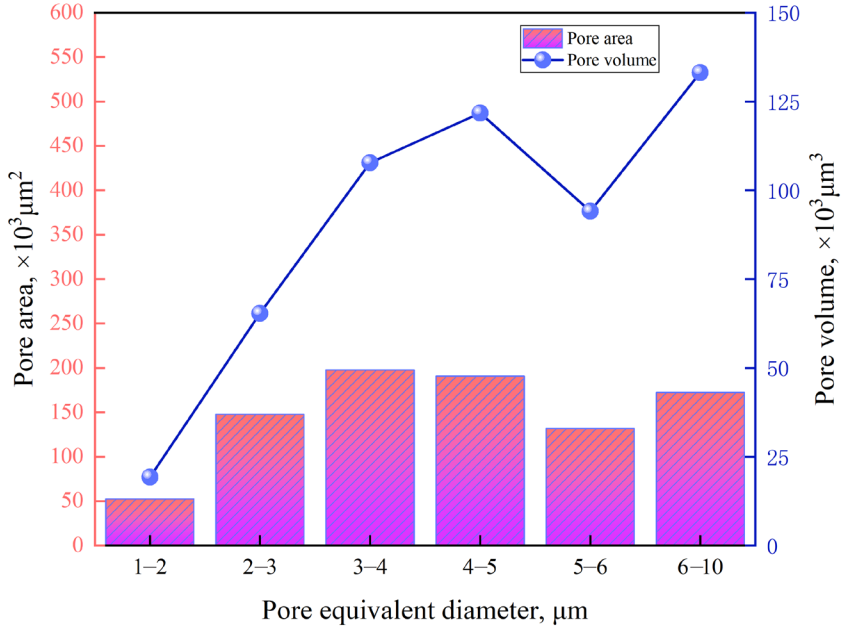

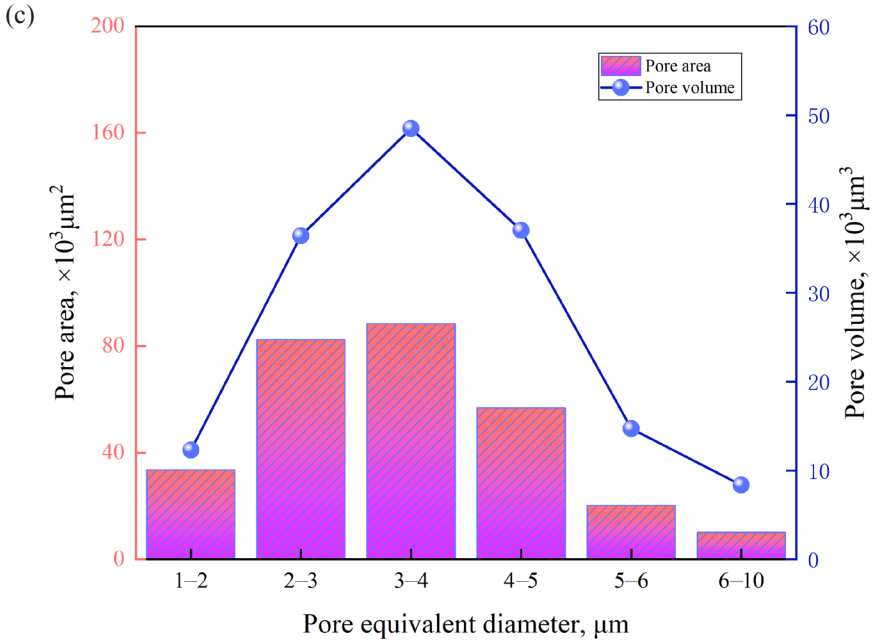

Fig. 12. Pore area and volume distribution of oil shale under different effective stresses: (a) 4 MPa, (b) 8 MPa, (c) 17 MPa.

With a slow increase in confining pressure, micro-fractures in oil shale close, and the porosity and permeability of the rock decrease rapidly. As confining pressure continues to increase, elastic deformation occurs in rock particles. The pores and throats in the rock become narrower with increasing overburden pressure, leading to a rapid reduction in rock porosity. Simultaneously, the narrowing of flow pathways increases fluid flow resistance within the rock, decreasing permeability. When the confining pressure exceeds the elastic yield stress of the rock, some rock particles may undergo plastic deformation and displacement, further occupying pore space. The channels connecting various pores may experience closure, local dissolution, recrystallization, or even compressive damage. Closed channels and fractured rock particles contribute to the generation of dead pores, further reducing rock porosity and permeability. However, due to the limited pore space, the rate of porosity and permeability reduction becomes relatively low. These factors collectively explain the changes in the experimental curves shown in Figure 4 and the variations in the experimental images in Figure 10 during the overburden loading process.

Combining the results from Figure 4 with the permeability of oil shale given in Figure 8, it is evident that lower permeability in oil shale corresponds to narrower permeation spaces. The pore structure becomes more complex, microscopic heterogeneity increases, and the connectivity between pores

weakens. Consequently, fewer effective flow channels can be established. As the permeability of rock is influenced by numerous factors, any minor rock deformation or structural damage will further reduce the number of effective flow channels, increasing the difficulty of fluid flow within the rock and intensifying the impact of overburden pressure on rock porosity and permeability. Therefore, the lower the core's permeability, the greater the loss caused by overburden pressure, including irreversible losses. Moreover, the extent of permeability loss is higher than that of porosity loss.

4. Conclusions

1. The porosity and permeability of an oil shale matrix exhibit exponential decreases with an increase in effective stress. Under the influence of effective stress, the mechanical compression of the oil shale matrix occurs with increasing stress. Consequently, the porosity of the oil shale matrix sharply decreases, leading to a reduction in permeability. Our three-dimensional visualization model aligned with experimental results. Under effective stress, pores were predominantly concentrated in the 3–5 μm equivalent diameter range, where the porosity and volume of pores in oil shale were most concentrated. However, under the high stress of 17 MPa, the area and volume of pores with larger diameters decreased significantly.
2. The porosity compressibility coefficient and stress sensitivity coefficient of oil shale varied in the two regions. The average porosity compressibility coefficient of the Fushun oil shale was 0.355 MPa^{-1}. Oil shale in this region exhibits relatively high initial porosity and compressibility coefficients. In contrast, the average porosity compressibility coefficient of the Xinjiang oil shale was 0.0105 MPa^{-1}.
3. In the Fushun region, oil shale was primarily characterized by matrix-type pores, with an average pore-permeability power exponent of 3.083. In contrast, the oil shale in Xinjiang exhibited a more complex pore structure, dominated by fracture-type pores, with an average pore-permeability power exponent of 9.469. The variation in γ-values indicates a rich and diverse pore structure within the rock.
4. Using the relationship between permeability compressibility, the stress sensitivity coefficient, and effective stress to describe the stress sensitivity of shale reservoirs, it was found that the permeability damage rate of oil shale increased sharply when the effective stress was less than 9 MPa. As the effective stress ranged between 9 and 16 MPa, the growth rate of damage decelerated slightly. However, after the effective stress exceeded 16 MPa, the rate of permeability damage tended to stabilize. When the effective stress was less than 8 MPa, the coefficient of stress sensitivity for permeability decreased significantly, reaching approximately 0.4 MPa^{-1}. However, once the effective stress surpassed 8 MPa, the curve of permeability stress sensitivity flattened gradually.

Acknowledgments

This study was supported by the Liaoning Province Applied Basic Research Program (grant No. 2022JH2/101300136) and the Liaoning Provincial Department of Education General Project (grants No. LJKZ0360, JYTMS20230821). We thank International Science Editing (http://www.internationalscienceediting.com) for editing this manuscript. The publication costs of this article were partially covered by the Estonian Academy of Sciences.

References

1. Järvik, O., Baird, Z. S., Rannaveski, R., Oja, V. Properties of kukersite shale oil. *Oil Shale*, 2021, **38**(4), 265–294.
2. Baird, Z. S., Oja, V., Järvik, O. Distribution of hydroxyl groups in kukersite shale oil: quantitative determination using Fourier transform infrared (FT-IR) spectroscopy. *Applied Spectroscopy*, 2015, **69**(5), 555–562.
3. Pikkor, H., Järvik, O., Lees, H., Konist, A., Siirde, A., Maaten, B. Characterization and enhancement of oil shale fly ash from CFB boiler. In: *2021 6th International Conference on Smart and Sustainable Technologies*, September 8–11, 2021, Bol and Split, Croatia. IEEE, 2021, 1–4.
4. Liu, Z., Ma, H., Wang, Z., Guo, Y., Li, W., Hou, Z. Experimental study on the thermophysical properties of Jimsar oil shale. *Oil Shale*, 2023, **40**(3), 194–211.
5. Zhao, L., Cheng, Y., Zhang, Y. Pore and fracture scale characterization of oil shale at different microwave temperatures. *Oil Shale*, 2023, **40**(2), 91–114.
6. Tan, X., Li, X., Liu, J., Zhang, L., Fan, Z. Study of the effects of stress sensitivity on the permeability and porosity of fractal porous media. *Physics Letters A*, 2015, **379**(39), 2458–2465.
7. Liu, Z., Yang, Y., Yao, J., Zhang, Q., Ma, J., Qian, Q. Pore-scale remaining oil distribution under different pore volume water injection based on CT technology. *Advances in Geo-Energy Research*, 2017, **1**(3), 171–181.
8. Wang, H., Ji, B., Lv, C., Zhang, L., Li, X., Cui, C., Yu, H., Nie, J. The stress sensitivity of permeability in tight oil reservoirs. *Energy Exploration & Exploitation*, 2019, **37**(4), 1364–1376.
9. Biot, M. A. General theory of three-dimensional consolidation. *Journal of Applied Physics*, 1941, **12**(2), 155–164.
10. Snow, D. T. Anisotropie permeability of fractured media. *Water Resources Research*, 1969, **5**(6), 1273–1289.
11. Jones Jr, F. O. A laboratory study of the effects of confining pressure on fracture flow and storage capacity in carbonate rocks. *Journal of Petroleum Technology*, 1975, **27**(01), 21–27.
12. McKee, C. R., Bumb, A. C., Koenig, R. A. Stress-dependent permeability and porosity of coal and other geologic formations. *SPE Formation Evaluation*, 1988, **3**(01), 81–91.

13. Liu, J., Liu, X. The effect of effective pressure on porosity and permeability of low permeability porous media. *Journal of Geomechanics*, 2001, **7**(1), 41–44 (in Chinese).
14. Chang, Z., Zhao, Y., Hu, Y. Theoretical and experimental studies of the coupling of seepage flow and 3D stresses in fractured rock masses. *Chinese Journal of Rock Mechanics and Engineering*, 2004, **23**(2), 4907–4911 (in Chinese).
15. Walsh, J. B. Effect of pore pressure and confining pressure on fracture permeability. *International Journal of Rock Mechanics and Mining Sciences*, 1981, **18**(5), 429–435.
16. Shi, Y., Wang, C. Y. Pore pressure generation in sedimentary basins: overloading versus aquathermal. *Journal of Geophysical Research: Solid Earth*, 1986, **91**(B2), 2153–2162.
17. Katsube, T. J., Mudford, B. S., Best, M. E. Petrophysical characteristics of shales from the Scotian shelf. *Geophysics*, 1991, **56**(10), 1681–1689.
18. Kwon, O., Kronenberg, A. K., Gangi, A. F., Johnson, B., Herbert, B. E. Permeability of illite-bearing shale: 1. Anisotropy and effects of clay content and loading. *Journal of Geophysical Research: Solid Earth*, 2004, **109**(B10).
19. Zheng, J., Zheng, L., Liu, H., Ju, Y. Relationships between permeability, porosity and effective stress for low-permeability sedimentary rock. *International Journal of Rock Mechanics and Mining Sciences*, 2015, **78**, 304–318.
20. Brower, K. R., Morrow, N. R. Fluid flow in cracks as related to low-permeability gas sands. *Society of Petroleum Engineers Journal*, 1985, **25**(02), 191–201.
21. Li, S., Tang, D., Pan, Z., Xu, H., Huang, W. Characterization of the stress sensitivity of pores for different rank coals by nuclear magnetic resonance. *Fuel*, 2013, **111**, 746–754.
22. Chalmers, G. R., Ross, D. J. K., Bustin, R. M. Geological controls on matrix permeability of Devonian Gas Shales in the Horn River and Liard basins, northeastern British Columbia, Canada. *International Journal of Coal Geology*, 2012, **103**, 120–131.
23. Ghanizadeh, A., Gasparik, M., Amann-Hildenbrand, A., Gensterblum, Y., Krooss, B. M. Experimental study of fluid transport processes in the matrix system of the European organic-rich shales: I. Scandinavian Alum Shale. *Marine and Petroleum Geology*, 2014, **51**, 79–99.
24. Gensterblum, Y., Ghanizadeh, A., Cuss, R. J., Amann-Hildenbrand, A., Krooss, B. M., Clarkson, C. R., Harrington, J. F., Zoback, M. D. Gas transport and storage capacity in shale gas reservoirs – a review. Part A: Transport processes. *Journal of Unconventional Oil and Gas Resources*, 2015, **12**, 87–122.
25. Meng, Y., Li, Z., Lai, F. Experimental study on porosity and permeability of anthracite coal under different stresses. *Journal of Petroleum Science and Engineering*, 2015, **133**, 810–817.
26. Jasinge, D., Ranjith, P. G., Choi, S. K. Effects of effective stress changes on permeability of Latrobe Valley brown coal. *Fuel*, 2011, **90**(3), 1292–1300.
27. Liu, H., Sang, S., Feng, Q., Hu, B., Hu, Y., Xu, H., Cheng, Q. Study on stress sensitivity of coal reservoir during drainage of coal-bed methane well in Southern

Qinshui Basin. *Journal of China Coal Society*, 2014, **39**(9), 1873–1878.
28. Chen, G., Qin, Y., Yang, Q., Li, W. Different stress sensitivity of different coal rank reservoir permeability and its effect on the coalbed methane output. *Journal of China Coal Society*, 2014, **39**(3), 504–509.
29. Peng, Y., Qi, Q., Deng, Z., Li, H. Experimental research on sensitivity of permeability of coal samples under confining pressure status based on scale effect. *Journal of China Coal Society*, 2008, **33**.
30. Ostensen, R. W. The effect of stress-dependent permeability on gas production and well testing. *SPE Formation Evaluation*, 1986, **1**(03), 227–235.
31. Li, M., Xiao, W. L., Guo, X., Zhang, L. H., Zheng, L. L. Laboratory study of the effective pressure law for permeability of the low-permeability sandstones from the Tabamiao area, Inner Mongolia. *Chinese Journal of Geophysics*, 2009, **52**(6), 1402–1413.
32. Dou, H., Zhang, H., Yao, S., Zhu, D., Sun, T., Ma, S., Wang, X. Measurement and evaluation of the stress sensitivity in tight reservoirs. *Petroleum Exploration and Development*, 2016, **43**(6), 1116–1123.
33. Feng, Y., Tang, H., Tang, H., Tang, H., Leng, Y., Shi, X., Liu, J., Wang, Z., Deng, C. Influence of geomechanics parameters on stress sensitivity in fractured reservoir. *Frontiers in Earth Science*, 2023, **11**, 1134260.
34. Chen, D., Pan, Z., Ye, Z. Dependence of gas shale fracture permeability on effective stress and reservoir pressure: model match and insights. *Fuel*, 2015, **139**, 383–392.
35. Zhao, X., Yang, Z., Wang, Z., Lin, W., Xiong, S., Luo, Y., Niu, Z., Xia, D. An experimental study on stress sensitivity of tight sandstones with different microfractures. *Advances in Civil Engineering*, 2020, **2020**, 1865464.
36. Guo, P., Deng, L., Liu, Q., Zhang, M., Wang, Z. Test and application of multiple stress sensitivity of low permeability gas reservoir. *Journal of Southwest Petroleum University (Science & Technology Edition)*, 2008, **30**(2), 78–82.
37. Xie, S., Jiao, C., He, S., Xie, Q., Gu, D., Zhu, H., Sun, L., Liu, H. An experimental study on stress-dependent sensitivity of ultra-low permeability sandstone reservoirs. *Acta Petrolei Sinica*, 2011, **32**, 489–494.
38. Kilmer, N. H., Morrow, N. R., Pitman, J. K. Pressure sensitivity of low permeability sandstones. *Journal of Petroleum Science and Engineering*, 1987, **1**(1), 65–81.
39. Wang, H., Liao, X., Lu, N., Cai, Z., Liao, C., Dou, X. A study on development effect of horizontal well with SRV in unconventional tight oil reservoir. *Journal of the Energy Institute*, 2014, **87**(2), 114–120.
40. Aybar, U., Yu, W., Eshkalak, M. O., Sepehrnoori, K., Patzek, T. Evaluation of production losses from unconventional shale reservoirs. *Journal of Natural Gas Science and Engineering*, 2015, **23**, 509–516.
41. Liao, J., Tang, H., Zhu, X., Li, G., Zhao, F., Lin, D. Study on stress sensitivity in ultra-low permeability sandstone reservoir of Chang 8 oil formation in Xifeng Oilfield based on microscopic methods. *Journal of China University of Petroleum*, 2012, **36**(2), 27–33.

42. Ruan, M., Wang, L. Low-permeability oilfield development and pressure-sensitive effect. *Acta Petrolei Sinica*, 2002, **23**(3), 73–76.
43. Vairogs, J., Hearn, C. L., Dareing, D. W., Rhoades, V. W. Effect of rock stress on gas production from low-permeability reservoirs. *Journal of Petroleum Technology*, 1971, **23**(09), 1161–1167.
44. David, C., Wong, T., Zhu, W., Zhang, J. Laboratory measurement of compaction-induced permeability change in porous rocks: implications for the generation and maintenance of pore pressure excess in the crust. *Pure and Applied Geophysics*, 1994, **143**, 425–456.
45. Zhao, H., Ning, Z., Zhao, T., Zhang, R., Wang, Q. Effects of mineralogy on petrophysical properties and permeability estimation of the Upper Triassic Yanchang tight oil sandstones in Ordos Basin, Northern China. *Fuel*, 2016, **186**, 328–338.
46. Mavko, G. M., Nur, A. The effect of nonelliptical cracks on the compressibility of rocks. *Journal of Geophysical Research: Solid Earth*, 1978, **83**(B9), 4459–4468.
47. Zhang, R., Ning, Z., Yang, F., Wang, X., Zhao, H., Wang, Q. Impacts of nanopore structure and elastic properties on stress-dependent permeability of gas shales. *Journal of Natural Gas Science and Engineering*, 2015, **26**, 1663–1672.
48. Zhang, R., Ning, Z., Yang, F., Zhao, H., Wang, Q. A laboratory study of the porosity-permeability relationships of shale and sandstone under effective stress. *International Journal of Rock Mechanics and Mining Sciences*, 2016, **81**, 19–27.
49. Zhang, W., Wang, Q., Ning, Z., Zhang, R., Huang, L., Cheng, Z. Relationship between the stress sensitivity and pore structure of shale. *Journal of Natural Gas Science and Engineering*, 2018, **59**, 440–451.
50. Wang, H., Ji, B., Lv, C., Zhang, L., Li, X., Cui, C., Yu, H., Nie, J. The stress sensitivity of permeability in tight oil reservoirs. *Energy Exploration & Exploitation*, 2019, **37**(4), 1364–1376.
51. Zhang, L., Wang, M., Shan, G., Pan, B. Experiment study on overburden porosity and permeability of volcanic rocks in Changling fault depression and its correction method. *World Geology*, 2022, **41**(01), 147–152 (in Chinese).
52. Huang, Q. *A Comparative Study on the Mechanical Strength and Pressure Pore Permeability of Different Coal Rank*. Master's thesis. Taiyuan University of Technology, Taiyuan, 2020 (in Chinese).
53. Yao, S., Dou, H., Chen, J., Ran, Q., Zhang, H., Ma, S. Discussion on the evaluation method standard of reservoir sensitivity flow experiment. *Technology Supervision in Petroleum Industry*, 2017, **33**(12), 26–29 (in Chinese).